

Luminosity dependence of the spatial and velocity distributions of galaxies: Semi-analytic models versus the Sloan Digital Sky Survey

Cheng Li^{1,2,3,4*}, Y.P. Jing^{1,4}, Guinevere Kauffmann², Gerhard Börner²,
 Xi Kang^{1,5}, Lan Wang^{6,2}

¹The Partner Group of MPI für Astrophysik, Shanghai Astronomical Observatory, Nandan Road 80, Shanghai 200030, China

²Max-Planck-Institut für Astrophysik, Karl-Schwarzschild-Strasse 1, 85748 Garching, Germany

³Center for Astrophysics, University of Science and Technology of China, Hefei, Anhui 230026, China

⁴Joint Institute for Galaxy and Cosmology (JOINGC) of SHAO and USTC

⁵Max-Planck-Institute for Astronomy, Königstuhl 17, D-69117 Heidelberg, Germany

⁶Department of Astronomy, Peking University, Beijing 100871, China

arXiv:astro-ph/0701218v3 18 Jan 2007

Accepted Received; in original form

ABSTRACT

By comparing semi-analytic galaxy catalogues with data from the Sloan Digital Sky Survey (SDSS), we show that current galaxy formation models reproduce qualitatively the dependence of galaxy clustering and pairwise peculiar velocities on luminosity, but some subtle discrepancies with the data still remain. The comparisons are carried out by constructing a large set of mock galaxy redshift surveys that have the same selection function as the SDSS Data Release Four (DR4). The mock surveys are based on two sets of semi-analytic catalogues presented by Croton et al. and Kang et al. . From the mock catalogues, we measure the redshift-space projected two-point correlation function $w_p(r_p)$, the power spectrum $P(k)$, and the pairwise velocity dispersion (PVD) in Fourier space $\sigma_{12}(k)$ and in configuration space $\sigma_{12}(r_p)$, for galaxies in different luminosity intervals. We then compare these theoretical predictions with the measurements derived from the SDSS DR4. On large scales and for galaxies brighter than L^* , both sets of mock catalogues agree well with the data. For fainter galaxies, however, both models predict stronger clustering and higher pairwise velocities than observed. We demonstrate that this problem can be resolved if the fraction of faint satellite galaxies in massive haloes is reduced by $\sim 30\%$ compared to the model predictions. A direct look into the model galaxy catalogues reveals that a significant fraction (15%) of faint galaxies ($-18 < M_{0.1} - 5 \log_{10} h < -17$) reside in haloes with $M_{vir} > 10^{13} M_\odot$, and this population is predominantly red in colour. These faint red galaxies are responsible for the high PVD values of low-luminosity galaxies on small scales.

Key words: galaxies: clustering - galaxies: distances and redshifts - large-scale structure of Universe - cosmology: theory - dark matter

1 INTRODUCTION

The spatial and velocity distributions of galaxies have long served as important probes of the cosmic density field. Studies of the two-point correlation function (2PCF) and the pairwise velocity dispersion (PVD), reveal how galaxies are related to the underlying mass distribution, thus providing strong tests for theoretical models of structure and galaxy formation (e.g. Peebles 1980; Davis et al. 1985).

Both the 2PCF and the PVD can be derived from redshift surveys of galaxies. The studies based on early surveys have established that the correlation function of L^* galaxies is close to a power law over nearly four orders of magnitude in amplitude (e.g. Peebles 1980). It has also been known for decades that the measured correlation of galaxies changes with luminosity (Xia et al. 1987; Börner et al. 1991; Loveday et al. 1995) and morphological type (e.g. Davis & Geller 1976). By taking advantage of the large redshift surveys assembled in recent years, in particular the two-degree Field Galaxy Redshift Sur-

* E-mail: leech@shao.edu.cn

vey (2dFGRS; Colless et al. 2001) and the Sloan Digital Sky Survey (SDSS; York et al. 2000), many authors have studied the dependence of clustering on a variety galaxy properties (Norberg et al. 2001, 2002; Zehavi et al. 2002; Budavári et al. 2003; Goto et al. 2003; Madgwick et al. 2003; Zehavi et al. 2005; Li et al. 2006a). These studies have revealed that galaxies with red colours, bulge-dominated morphologies and spectral types indicative of old stellar populations reside preferentially in dense regions. Furthermore, luminous (massive) galaxies cluster more strongly than less luminous (less massive) galaxies, with the luminosity (mass) dependence becoming more pronounced for galaxies brighter than L^* (the characteristic luminosity of the Schechter (1976) function).

Measurements of the PVD have also been carried out by many authors, either by modelling the redshift distortion of the 2PCF (Davis & Peebles 1983; Mo et al. 1993; Fisher et al. 1994; Zurek et al. 1994; Marzke et al. 1995; Somerville et al. 1997), or by measuring the redshift-space power spectrum (Jing & Börner 2001a). The early results often varied significantly from one survey to another (Mo et al. 1993). The PVD of galaxies in the local Universe was not well established until the work of Jing et al. (1998) on the Las Companas Redshift Survey. These results have now been confirmed by (Zehavi et al. 2002, 2005) using the SDSS and by Hawkins et al. (2003) using the 2dFGRS. Jing & Börner (2004) (hereafter JB04) presented the first determination of the PVD for galaxies in different luminosity intervals. This analysis led to the discovery that the PVD exhibits a non-monotonic dependence on galaxy luminosity, in that the value of σ_{12} measured at $k = 1 \text{ hMpc}^{-1}$ decreases as a function of increasing luminosity for galaxies fainter than L^* , but increases again for the most luminous galaxies in the sample. Since the PVD is an indicator of the depth of the local gravitational potential, this discovery implies that a significant fraction of faint galaxies are located in massive dark matter haloes that host galaxy groups and clusters, but that the majority of L^* galaxies are located in galactic scale haloes. These results were recently confirmed by Li et al. (2006b) (hereafter Paper II) using the second data release (DR2) of the SDSS. These authors considered their results in conjunction with the observed luminosity and color dependences of the two-point correlation function (Li et al. 2006a) (hereafter Paper I) and concluded that the faint red galaxy population located in rich clusters was likely to be responsible for the high PVD values for low-luminosity galaxies on small scales.

A quantitative understanding of the luminosity dependence of the PVD requires a model linking the properties of galaxies to the dark matter haloes in which they are found. One approach is to carry out N-body plus hydrodynamical simulations (e.g. Katz & Gunn 1991; Cen & Ostriker 1993; Bryan et al. 1994; Navarro & White 1994; Couchman et al. 1995; Thoul & Weinberg 1995; Abel et al. 1997; Weinberg et al. 1998; Yoshikawa et al. 2000; Springel et al. 2001). By numerically solving the gravitational and hydrodynamical equations, galaxy formation in an expanding universe can be simulated in a straightforward way. However, the limited dynamic range in current hydro/N-body simulations and the limited understanding of important physical processes such as star formation and supernova feedback mean that the hydrodynamical simula-

tions do not in general reproduce the observed galaxy luminosity function (e.g. Nagamine et al. 2004). As a result, these simulations cannot be used to interpret the PVD.

Another method is the Halo Occupation Distribution (HOD) approach, which aims to provide a statistical description of how dark matter haloes are populated by galaxies (e.g. Jing et al. 1998; Peacock & Smith 2000; Seljak 2000; Sheth et al. 2001; Berlind & Weinberg 2002; Kang et al. 2002; Cooray & Sheth 2002). In a typical HOD model, the link between galaxies and dark matter haloes is expressed in terms of the halo occupation function $P(N|M)$, which gives the probability that a halo of mass M contains N galaxies in a given luminosity range. In addition, the HOD model must specify the spatial distribution of the galaxies within individual haloes. An alternative way of describing this link is in terms of the conditional luminosity function $\Phi(L|M)$ (CLF, Yang et al. 2003), which characterises the luminosity distribution of galaxies that reside in a halo of mass M . The HOD approach has been used to interpret the observed dependence of clustering on properties such as luminosity, colour, morphology and spectral type (e.g. Yang et al. 2003, 2004; van den Bosch et al. 2003; Yan et al. 2003, 2004; Zehavi et al. 2005; Cooray 2006).

JB04 used the HOD models of Yang et al. (2003) to construct mock galaxy catalogues from N-body simulations. These catalogues were used to compare the predicted PVD with the observations. They found that while the model provided a successful match to the luminosity function as well as the luminosity dependence of the clustering on large scales, it was unable to reproduce the non-monotonic luminosity dependence of the PVD (see Figs. 8 and 9 of JB04 and Fig. 7 of Paper II). Recently, Slosar et al. (2006) used their own HOD models to show that the non-monotonic behaviour can be recovered if a sufficient number of the faint galaxies are satellite galaxies in high mass haloes. More recent studies by Tinker et al. (2006) and van den Bosch et al. (2006) also support this interpretation. All these studies indicate that the luminosity dependence of the PVD can provide a strong constraint on theories of galaxy formation.

A third method is to construct semi-analytical models (SAMs) of galaxy formation (e.g. White & Frenk 1991; Lacey & Silk 1991; Kauffmann et al. 1993, 1997, 1999; Cole et al. 1994, 2000; Somerville & Primack 1999). This method incorporates parametrised models to describe the physical processes that regulate how stars form in galaxies as a function of cosmic time. The model parameters are chosen to reproduce key observational quantities, such as the luminosity functions of galaxies in various wavebands, the colour-magnitude relation for early-type galaxies, and the Tully-Fisher relation for spiral galaxies. Semi-analytic models represent a powerful way of predicting the observed properties of galaxies.

Two recent SAMs have been presented by Kang et al. (2005) (hereafter K05) and Croton et al. (2006) (hereafter C06). Both models are based on high-resolution N -body simulations and successfully match a variety of observational results. The model galaxy catalogues provided by these authors contain information not only about galaxy distributions in phase space, but also about the observed properties of individual galaxies (e.g. the absolute magnitudes in the five photometric pass-bands of the SDSS). In this paper, we use these semi-analytic catalogues to study whether the lu-

minosity dependence of the 2PCF and the PVD of galaxies in the local Universe can be reproduced in these models.

As discussed in Jing et al. (1998), a large set of mock samples is essential for this comparison. The mock samples can be used to quantify the errors resulting from “cosmic variance” effects and and from systematics in the estimation methods (e.g. the uncertainties in the distribution function of peculiar velocities and in the mean infall velocities of galaxy pairs). In this paper, we construct our mock galaxy catalogues that have the same selection effects as the SDSS Data Release Four (DR4, Adelman-McCarthy et al. 2006). To take into account the effect of the cosmic variance, we construct 10 mock catalogues for each SAM in which the observer is placed at different, randomly chosen positions within the simulation box. Using these mock catalogues and the same estimation methods used in Papers I and II, we measure the redshift-space projected 2PCF $w_p(r_p)$, the real-space power spectrum $P(k)$ and the PVD $\sigma_{12}(k)$ for galaxies in different luminosity intervals.

Observational results from the SDSS have already been presented in Papers I and II, using a sample of $\sim 200,000$ galaxies drawn from the SDSS Data Release Two (DR2). Here we re-compute all the clustering statistics using the SDSS DR4 in order to take advantage of the larger number of galaxies in the newer release. We also measure $\sigma_{12}(r_p)$, the PVD in configuration space, in order to make comparisons with recent HOD models of Slosar et al. (2006) and Tinker et al. (2006).

In the following sections we describe the observational measurements (§2), the procedure for constructing mock catalogues (§3), the comparison between models and observations (§4), the mock experiments to bring the models into better agreement with the data (§5), and the nature of the luminosity dependence of the PVD (§6). In §7, we summarise our results, discuss the implications for the models, and suggest possible improvements both for future observations and models.

Throughout this paper, we assume a cosmological model with the density parameter $\Omega_0 = 0.3$ and cosmological constant $\Lambda_0 = 0.7$. In the C06 SAM model, the cosmological parameters are slightly different from these adopted values. To properly compare this model with the observations, we calculate the positions, redshifts, and apparent magnitudes for mock galaxies using the C06 cosmological parameters. In the analysis of mock galaxy clustering, we use the same cosmological parameters as in the analysis of the observational clustering. A Hubble constant $h = 1$, in units of $100 \text{ km s}^{-1} \text{Mpc}^{-1}$, is assumed throughout this paper when computing absolute magnitudes.

2 OBSERVATIONAL MEASUREMENTS

2.1 Samples

The SDSS is the most ambitious optical imaging and spectroscopic survey to date. The survey goals are to obtain photometry of a quarter of the sky and spectra of nearly one million objects. Imaging is obtained in the u , g , r , i , z bands (Fukugita et al. 1996; Smith et al. 2002; Ivezić et al. 2004) with a special purpose drift scan camera (Gunn et al. 1998) mounted on the SDSS 2.5 meter

Table 1. Luminosity samples selected from the NYU-VAGC Sample dr4.

SAMPLE	$M_{0.1r}$		NUMBER OF GALAXIES
	RANGE	MEDIAN	
L1.....	[−18.0, −17.0)	-17.59	7090
L2.....	[−18.5, −17.5)	-18.09	11992
L3.....	[−19.0, −18.0)	-18.59	20571
L4.....	[−19.5, −18.5)	-19.11	38203
L5.....	[−20.0, −19.0)	-19.58	66737
L6.....	[−20.5, −19.5)	-20.05	98589
L7.....	[−21.0, −20.0)	-20.52	121822
L8.....	[−21.5, −20.5)	-20.95	113449
L9.....	[−22.0, −21.0)	-21.38	70499
L10.....	[−22.5, −21.5)	-21.80	27427
L11.....	[−23.0, −22.0)	-22.22	6085

telescope (Gunn et al. 2006) at Apache Point Observatory. The imaging data are photometrically (Hogg et al. 2001; Tucker et al. 2006) and astrometrically (Pier et al. 2003) calibrated, and used to select spectroscopic targets for the main galaxy sample (Strauss et al. 2002), the luminous red galaxy sample (Eisenstein et al. 2001), and the quasar sample (Richards et al. 2002). Spectroscopic fibres are assigned to the targets using an efficient tiling algorithm designed to optimise completeness (Blanton et al. 2003c). The details of the survey strategy can be found in York et al. (2000) and an overview of the data pipelines and products is provided in the Early Data Release paper (Stoughton et al. 2002). More details on the photometric pipeline can be found in Lupton et al. (2001).

Papers I and II presented the measurements of the redshift-space projected 2PCF $w_p(r_p)$, the real-space power spectrum $P(k)$ and the PVD $\sigma_{12}(k)$ for different classes of galaxies. In those papers, we used the New York University Value Added Catalogue (NYU-VAGC)¹, which is a catalogue of local galaxies (mostly below $z \approx 0.3$) constructed by Blanton et al. (2005) based on the SDSS DR2. Here we use a new version of the NYU-VAGC (Sample dr4), which is based on SDSS DR4, to re-determine these statistics, but as a function of luminosity only. The NYU-VAGC is described in detail in Blanton et al. (2005).

From Sample dr4, we construct 11 luminosity subsamples, as listed in Table 1. We select all objects with $14.5 < r < 17.6$ that are identified as galaxies in the Main sample (note that r -band magnitude has been corrected for galactic extinction). We also restrict the galaxies to the redshift range $0.01 \leq z \leq 0.3$, and the absolute magnitude range $-23 < M_{0.1r} < -17$. Here, $M_{0.1r}$ is the r -band absolute magnitude corrected to its $z = 0.1$ value using the K -correction code of Blanton et al. (2003a) and the luminosity evolution model of Blanton et al. (2003b). The resulting sample includes a total of 292,782 galaxies, which are then divided into subsamples according to absolute magnitude. Each subsample includes galaxies in an absolute magnitude interval of 1 magnitude, with successive subsamples overlapping by 0.5 magnitude. This sample selection is identical to

¹ <http://wassup.physics.nyu.edu/vagc/>

that in Paper I, except that we have adopted slightly different apparent and absolute magnitudes limits. We do not consider galaxies fainter than $M_{0.1r} = -17$, because the volume covered by such faint samples are very small and the results are subject to large errors from cosmic variance (see for example Fig. 6 of Paper I). The faint apparent magnitude limit of 17.6 is chosen to yield a uniform galaxy sample that is complete over the entire area of the survey.

2.2 Methods

Our methodology for computing $w_p(r_p)$, $P(k)$ and $\sigma_{12}(k)$ in the SDSS has been described in detail in Papers I and II. We present below a brief description and the reader is referred to the earlier papers for details.

For each subsample, the redshift-space 2PCF $\xi^s(r_p, \pi)$ is measured using the Hamilton (1993) estimator. The redshift-space projected 2PCF $w_p(r_p)$ is then estimated by integrating $\xi^s(r_p, \pi)$ along the line-of-sight direction π with $|\pi|$ ranging from 0 to $40 h^{-1}$ Mpc. Random samples are constructed in which the redshift selection function is explicitly modelled using the observed luminosity function. We have also corrected carefully for the effect of fibre collisions (see (Li et al. 2006c, hereafter Paper III) for a detailed description).

From $\xi^s(r_p, \pi)$, we obtain for each subsample the redshift-space power spectrum $P^{(s)}(k, \mu)$. We then determine simultaneously the power spectrum $P(k)$ and the PVD $\sigma_{12}(k)$ by modelling the measured $P^{(s)}(k, \mu)$ using the relation

$$P^{(s)}(k, \mu) = P(k)(1 + \beta\mu^2)^2 \frac{1}{1 + (k\mu\sigma_{12}(k))^2}. \quad (1)$$

Here k is the wavenumber, μ the cosine of the angle between the wavevector and the line of sight, and β the linear redshift distortion parameter. In the equation above, the first term is the power spectrum, the second term is the Kaiser linear compression effect (Kaiser 1987), and the third term is the damping effect caused by the random motion of the galaxies. In the computation, we have fixed the linear redshift distortion parameter $\beta = 0.45$. As we have shown in Paper II, our $\sigma_{12}(k)$ measurements are robust to reasonable changes of the β values.

In addition, we also compute the configuration space PVD, $\sigma_{12}(r_p)$, which is estimated by modelling redshift distortions in the 2PCF. This method relies on the fact that the peculiar motions of galaxies change only their radial distances in redshift space. Thus the information for peculiar velocities along the line of sight can be recovered by modelling the redshift-space 2PCF $\xi^s(r_p, \pi)$ as a convolution of the real-space 2PCF $\xi(r)$ with the distribution function of the pairwise velocity $f(v_{12})$:

$$\xi^s(r_p, \pi) = \int f(v_{12}) \xi \left(\sqrt{r_p^2 + (\pi - v_{12})^2} \right) dv_{12}, \quad (2)$$

where $v_{12} = v_{12}(r_p, \pi)$ is the pairwise peculiar velocity. The real-space correlation function $\xi(r)$ is inferred from the projected 2PCF $w_p(r_p)$, which is a simple Abel transform of $\xi(r)$. An exponential form is adopted for $f(v_{12})$:

$$f(v_{12}) = \frac{1}{\sqrt{2}\sigma_{12}} \exp \left(-\frac{\sqrt{2}}{\sigma_{12}} |v_{12} - \bar{v}_{12}| \right) \quad (3)$$

where \bar{v}_{12} is the mean and σ_{12} is the dispersion of the one-dimensional peculiar velocities. Assuming the infall model for \bar{v}_{12} used by Jing et al. (1998), the PVD is then estimated as a function of the projected separation r_p by comparing the observed $\xi^{(s)}(r_p, \pi)$ with the modelled one.

2.3 Results

Using the samples listed in Table 1 and the methods described above, we have derived the the projected 2PCF $w_p(r_p)$, the power spectrum $P(k)$, the PVD in Fourier space $\sigma_{12}(k)$, and the PVD in configuration space $\sigma_{12}(r_p)$. The results are shown in Figure 1. Panels from left to right correspond to the six luminosity subsamples (samples L1, L3, L5, L7, L9 and L11 in Table 1), while panels from top to bottom correspond to the different clustering statistics. The blue and red lines compare the results obtained from the DR4 and DR2. The two data releases agree quite well, except for $\sigma_{12}(k)$ in the brightest luminosity sample, where the DR4 measurements on scales $k > 0.5 h\text{Mpc}^{-1}$ are larger, but still within the error bars of the DR2 measurements.

A comparison of the PVD for the two different estimation methods is shown in Figure 2 for all 11 luminosity samples. The k -space measurements $\sigma_{12}(k)$ are plotted in black. The PVDs in configuration space $\sigma_{12}(r_p)$ are plotted in red as a function of $1/r_p$ and in blue as a function of π/r_p . We see that, if the relation $k = 1/r_p$ is used in the comparison, $\sigma_{12}(r_p)$ and $\sigma_{12}(k)$ agree well within error bars both in shape and in amplitude, for galaxies fainter than -19 or brighter than -21 . For galaxies around L^* , $\sigma_{12}(r_p)$ is systematically higher than $\sigma_{12}(k)$, by up to 30 per cent on intermediate scales. Using π/r_p for k does not improve the agreement between the two quantities. It is not surprising that there are differences between the results, because the PVD $\sigma(r)$ in 3D configuration space is not a constant. Our results indicate that it is important that the PVDs from the semi-analytic model be computed in exactly the same manner as is done in the observations.

3 MOCK CATALOGUES

3.1 SAMs and model catalogues

In this paper, we compare the clustering and velocity statistics predicted by the semi-analytic models with the observations by constructing a large set of mock galaxy samples that have the same selection effects as the SDSS DR4. We use two sets of semi-analytic catalogues of galaxies at $z = 0$, provided by C06 and K05, to construct our mock catalogues.

The semi-analytic catalogues of C06 were constructed using the Millennium Run (Springel et al. 2005), a very large simulation of the concordance ΛCDM cosmogony with 10^{10} particles. The relevant cosmological parameters are the density parameter $\Omega_m = 0.25$, the cosmological constant $\Omega_\Lambda = 0.75$, and the amplitude of the power spectrum $\sigma_8 = 0.9$. The chosen simulation volume is a periodic box of size $L_{box} = 500 h^{-1}$ Mpc on a side, which implies a particle mass of $8.6 \times 10^8 h^{-1}\text{M}_\odot$. After finding haloes and subhaloes at all output snapshots and building merging trees that describe how haloes grow as the universe

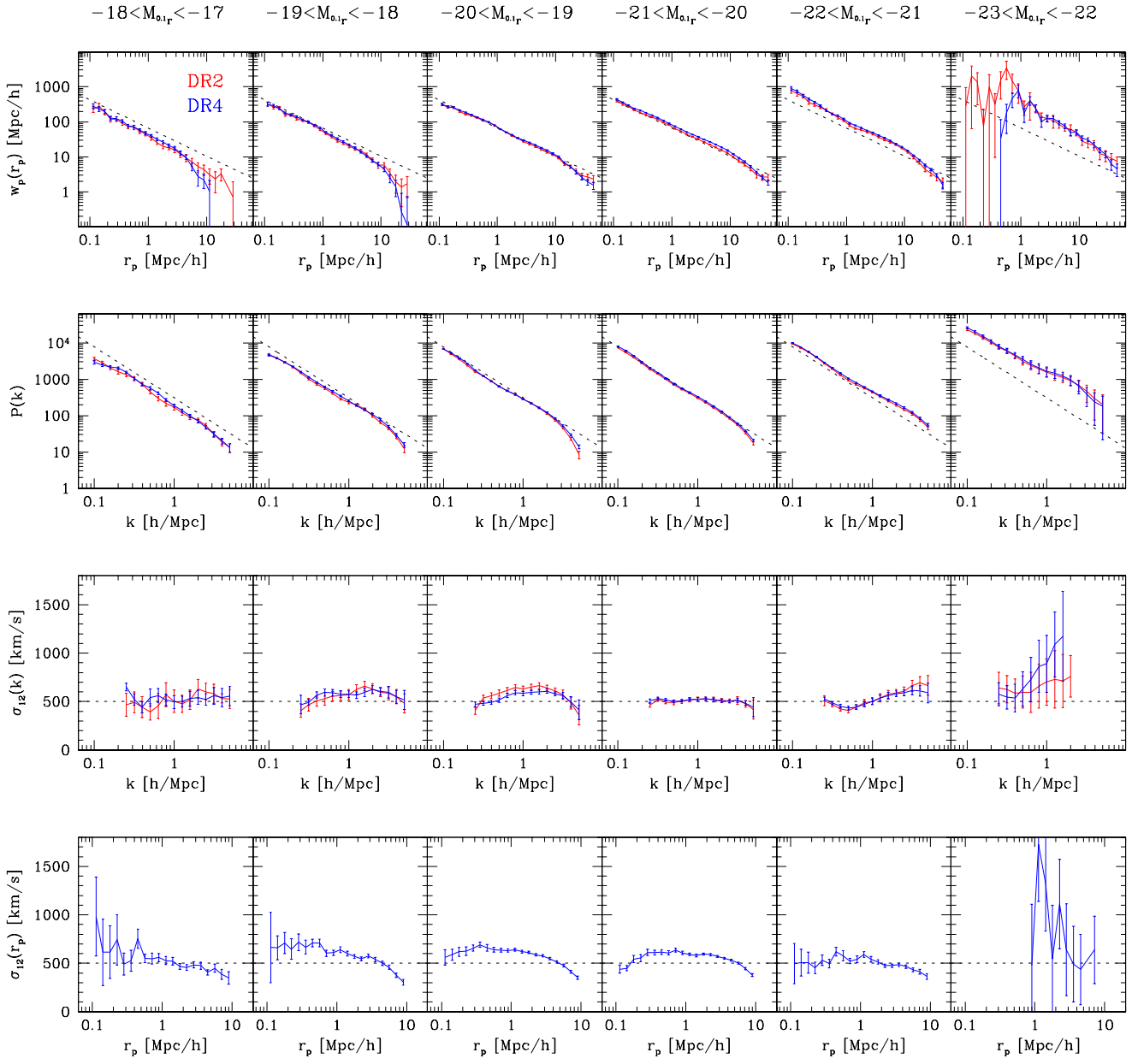


Figure 1. Clustering and velocity statistics for galaxies with various luminosities. Panels from left to right correspond to different luminosity intervals, as indicated at the top of the figure. Panels from top to bottom correspond to different statistics: the projected 2PCF $w_p(r_p)$, the real space power spectrum $P(k)$, the PVD measured in Fourier space $\sigma_{12}(k)$, and the PVD in configuration space $\sigma_{12}(r_p)$. Blue and red lines are measured from the SDSS DR4 and the SDSS DR2 respectively. The dashed lines are plotted for reference, which are the same in each row (from top to bottom): the line corresponding to $\xi(r) = (r/5h^{-1}\text{Mpc})^{-1.8}$, the power spectrum $P(k) = (60/k)^{1.4}$, and (in both the bottom two rows) the line for $\sigma_{12} = 500 \text{ km s}^{-1}$.

evolves, C06 implemented a model to simulate the formation and evolution of galaxies and their central supermassive black holes. Their model closely matches many observations, including the galaxy luminosity function, galaxy colour distributions, the Tully-Fisher relation of spirals, the colour-magnitude relation of ellipticals, the bulge mass-black hole mass relation, and the volume-averaged cosmic star formation rate. The models yield a number of useful quantities that can be directly compared with observations at different redshifts. These include positions in

phase space, total luminosities and bulge luminosities in various bands, stellar masses, cold, hot and ejected gas mass, black hole mass, and star formation rate. The semi-analytic galaxy catalogue used here is publicly available at <http://www.mpa-garching.mpg.de/galform/agnpaper> and it includes a total of $\sim 9 \times 10^6$ galaxies at redshift zero in the full simulation box. The catalogue is complete down to $M_r - 5 \log h = -16.6$ and to $M_B - 5 \log h = -15.6$.

Using the semi-analytical approach, K05 also carried out a set of semi-analytic galaxy catalogues by modelling

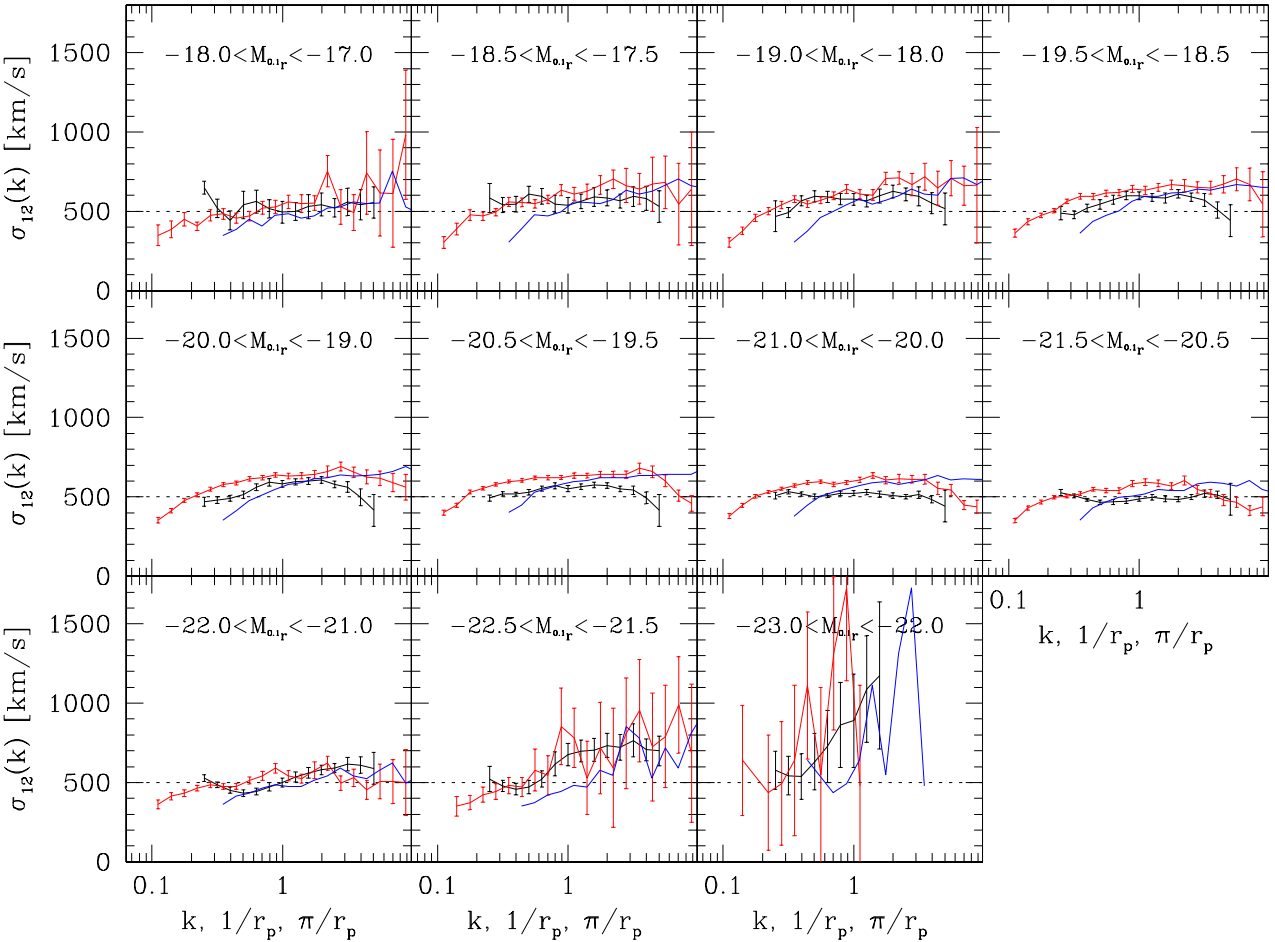


Figure 2. Comparison of PVD as measured in Fourier space and in configuration space for galaxies in different luminosity intervals, as indicated in each panel. Black lines plot σ_{12} as a function of k . The PVDs measured in configuration space are plotted in red as a function of $1/r_p$ and in blue as a function of π/r_p . The dashed line in each panel represents the PVD value of 500 km s^{-1} .

galaxy formation in a series of high-resolution N -body simulations. The simulations used in their study have been carried out with the vectorised parallel P³M code (Jing & Suto 2002), considering boxes with periodic boundary conditions in a concordance Λ CDM cosmology. The cosmological parameters $\Omega_m = 0.3$ and $\Omega_\lambda = 0.7$ are slightly different from those of C06. There are 512^3 particles in the simulation box of $L_{box} = 100 h^{-1} \text{Mpc}$ (L_{100} simulation). Although the simulation is much smaller than that of C06, the mass resolution is comparable. The galaxy formation model has been updated to include supermassive black hole formation and AGN energy feedback, as described in Kang et al. (2006). The SAM model of K05 can also match many observations, e.g. the luminosity functions of galaxies in various wavebands redder than the u -band, the main features in the observed colour distribution of galaxies, the colour-magnitude relation for elliptical galaxies in clusters, the metallicity-luminosity relation and metallicity-rotation velocity relation of spiral galaxies, and the gas fraction in present-day spiral galaxies.

In order to study the clustering of galaxies on large scales, we will use a simulation of 512^3 particles and box size $300 h^{-1} \text{Mpc}$ (L_{300} simulation) with the same cosmological

parameters as the smaller box. Because of its poor mass resolution, we do not follow the formation histories of galaxies in this simulation. Instead, we combine the L_{100} simulation and a set of resimulations of massive clusters of $\sim 10^{15} M_\odot$ (see K05), and use these higher resolution simulations to populate the dark matter halos in the L_{300} simulation. In detail, for each halo in the L_{300} simulation, we select an halo from the L_{100} simulation or the cluster resimulations that is closest in mass. The galaxies of this matching halo will be placed into the L_{300} simulation halo. All physical properties as well as the relative position and velocity with respect to centre of halo mass are kept the same.

The Kang et al. and C06 are similar, but there are still many differences in the details of the implementation. For example, C06 allowed starbursts to be triggered during minor mergers. The energy released by gas accretion onto the central supermassive black hole is also slightly different in the two implementations. The parameters of the star formation laws and even of the cosmological models are different. These differences make it interesting for us to compare the clustering of galaxies in the two SAM implementations.

Figure 3 shows the $0.1r$ -band luminosity function for galaxies in the semi-analytical catalogues, compared to

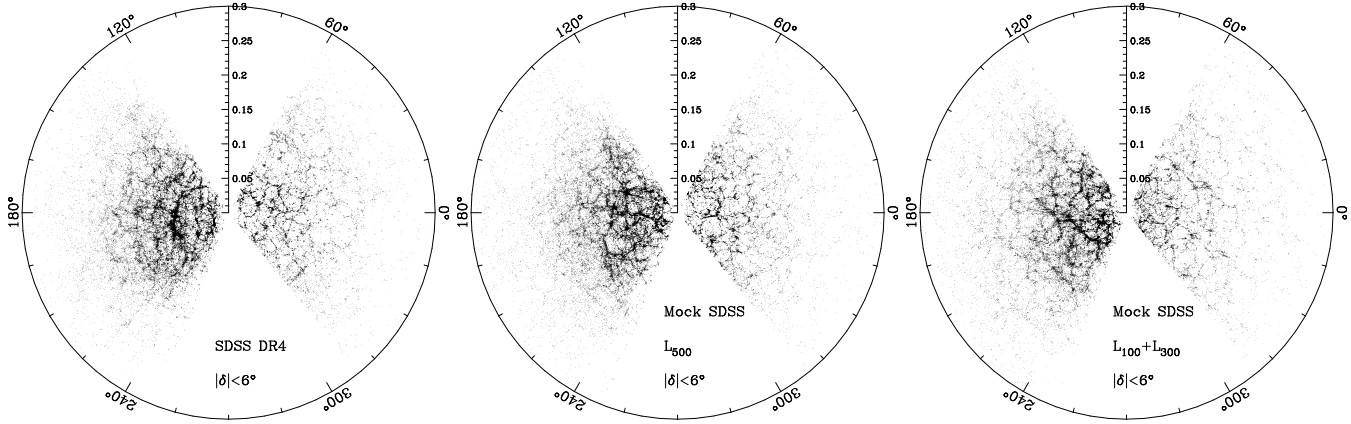


Figure 4. Equatorial distribution of right ascension and redshift for galaxies within 6° of the equator in the SDSS (left) and in our mock catalogues.

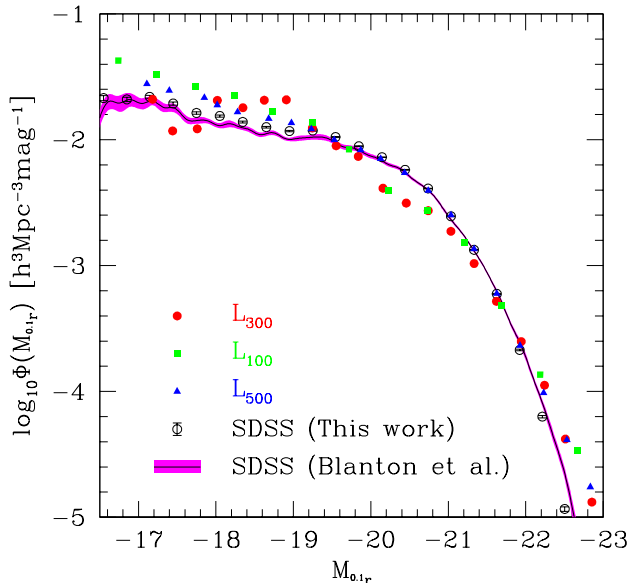


Figure 3. Galaxy luminosity function at $0.1r$ -band. Triangles are for the L_{500} SAM catalogue of Croton et al. (2006). Squares and filled circles are respectively for the L_{100} and L_{300} catalogues of Kang et al. (2005). The line surrounded by the magenta band plots the observational result presented by Blanton et al. (2003b) based on the first data release of the SDSS; the magenta band indicates its error. Open circles with error bars represent the result obtained in this paper with the SDSS DR4.

the SDSS observations presented in Blanton et al. (2003b). The SAMs reproduce the observed luminosity function reasonably well, although they still predict too many faint ($M_{0.1r} > -19$) and bright ($M_{0.1r} < -22$) galaxies. It is worth noting that the L_{100} and L_{300} catalogues contain fewer L^* galaxies than observed.

We have also recomputed the observed galaxy luminosity function using our SDSS DR4 sample. We have corrected for the volume incompleteness by weighting each galaxy by a factor of $V_{\text{survey}}/V_{\max}$, where V_{survey} is the volume of the sample and V_{\max} is the maximum volume over which the galaxy could be observed within the redshift range and the apparent magnitude range of the sample. To determine

the V_{\max} , we have used the `kcorrect` code of Blanton et al. (2003a) to compute for each galaxy a z_{\min} and a z_{\max} , the redshifts at which the galaxy would reach the bright and the faint r -band magnitude limits. Our measurement is also shown in Figure 3, and it agrees quite well with the result of Blanton et al. (2003b). The errors are estimated using the bootstrap resampling technique (Barrow et al. 1984).

3.2 Constructing mock galaxy redshift surveys

We aim to construct mock galaxy redshift surveys that have the same observational selection effects as the SDSS DR4. A detailed account of the observational selection effects accompanies with the NYU-VAGC release. Our methodology of constructing mock SDSS catalogues has been described in detail in Paper III. First, we create $n \times n \times n$ replications of the simulation box which has periodic boundary conditions, and place a virtual observer randomly within the central box. Here n is chosen so that the required depth can be achieved in all directions for the observer. Next, we define a (α, δ) -coordinate frame and remove all galaxies that lie outside the survey region. We then compute for each galaxy the redshift as "seen" by the observer, the r -band apparent magnitude and $M_{0.1r}$, the r -band absolute magnitude of the galaxy at $z = 0.1$. Finally, we mimic the position-dependent completeness by randomly eliminating galaxies using the completeness masks provided in the `Sample dr4`.

We produce 10 mock catalogues from each SAM catalogue, from which we then select luminosity samples in the same way as the real sample. As pointed out by Yang et al. (2004), the L_{300} catalogue is only complete down to $M_{b,J} \approx -18.4$ (i.e. $M_{0.1r} \approx -19.3$), while the L_{100} catalogue is complete down to $M_{b,J} \approx -14$ (i.e. $M_{0.1r} \approx -14.9$) because it is based on higher-resolution simulation. This implies that the mock samples constructed from the L_{300} catalogue would be incomplete out to a distance of $\sim 350 h^{-1} \text{Mpc}$. To overcome this problem, we combined the L_{100} and L_{300} mock samples by selecting galaxies with $M_{0.1r} < -19$ from the L_{100} samples and selecting those with $M_{0.1r} > -19$ from the L_{300} ones.

In total we have 20 mock catalogues: 10 from the L_{500} catalogue and 10 from the L_{100} plus L_{300} catalogues. Figure 4 shows the equatorial distribution of galaxies in one

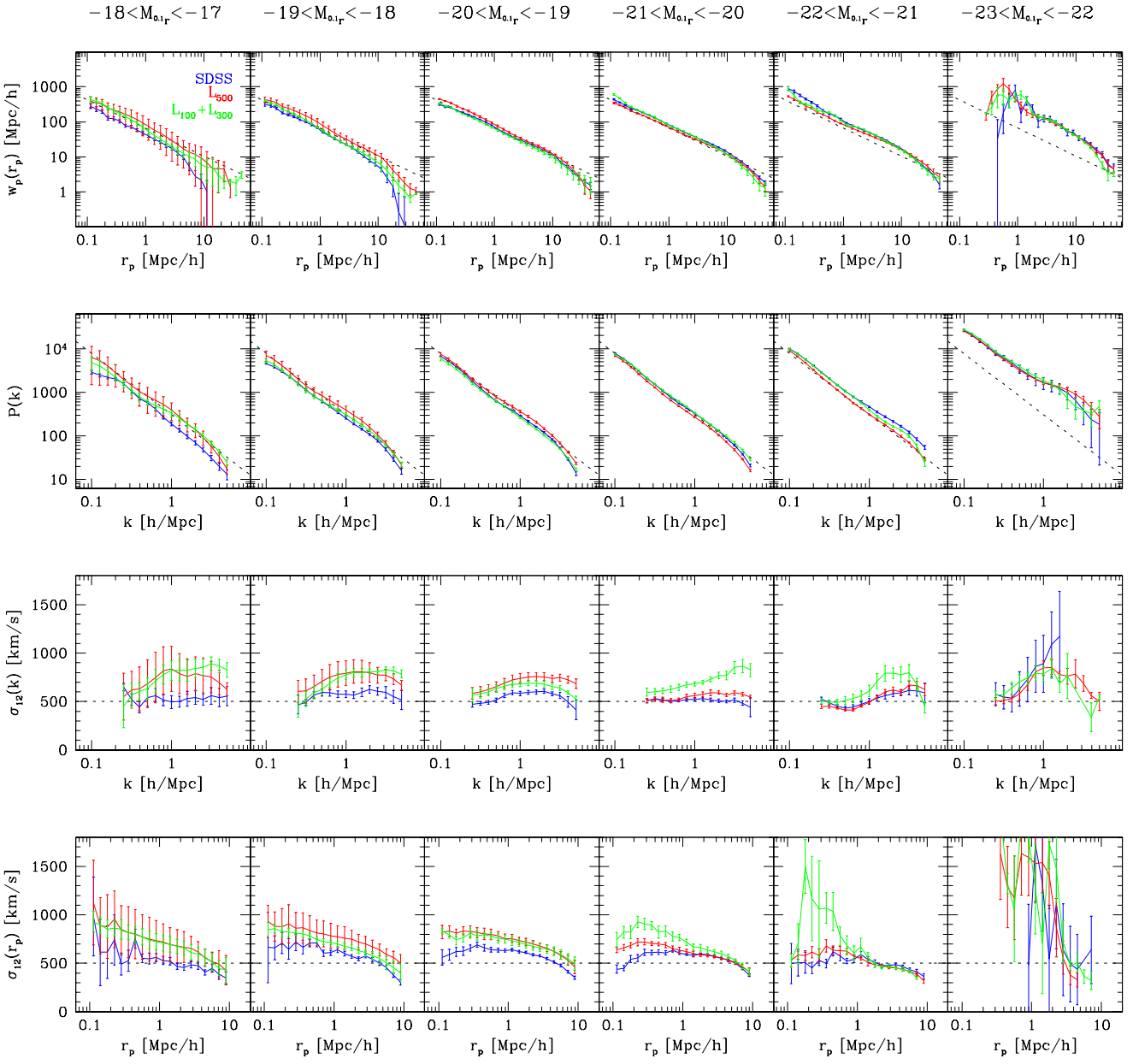


Figure 5. Comparison of the clustering and velocity statistics as measured from mock catalogues and as observed from SDSS DR4, for galaxies with various luminosities. Panels from left to right correspond to different luminosity intervals, as indicated above the top panels. Panels from top to bottom correspond to different statistics: $w_p(r_p)$, $P(k)$, $\sigma_{12}(k)$ and $\sigma_{12}(r_p)$. Red and green lines represent the average measurement from the L_{500} and the $L_{100} + L_{300}$ mock samples respectively. The error bars indicate the uncertainty due to cosmic variance as estimated from 10 different mock catalogues. Blue lines plot the observational results. The dashed lines are the same as in Figure 1.

of the L_{500} mock catalogues (middle) and in one of the $L_{100} + L_{300}$ catalogues (right), compared to the real sample (left). The numbers of galaxies in our L_{500} mock catalogues, 300,000 on average with a dispersion of ~ 7000 , are consistent with the observational sample. In case of $L_{100} + L_{300}$, however, the numbers are smaller: 250,000 on average with a dispersion of ~ 3700 . As can be seen from Figure 3, the model of K05 predicts fewer L^* galaxies than the observations.

4 COMPARISONS BETWEEN MODELS AND OBSERVATIONS

For each mock sample, we measure $w_p(r_p)$, $P(k)$, $\sigma_{12}(k)$ and $\sigma_{12}(r_p)$ using the same method as for the observational samples (§ 2). Figure 5 shows the results in six luminosity intervals, the same as in Figure 1. In each panel, the average measurement is plotted in red for the L_{500} mock samples and in green for the $L_{100} + L_{300}$ samples. The error bars indicate the uncertainty due to cosmic variance as estimated from 10 different mock samples. For comparison, the observational

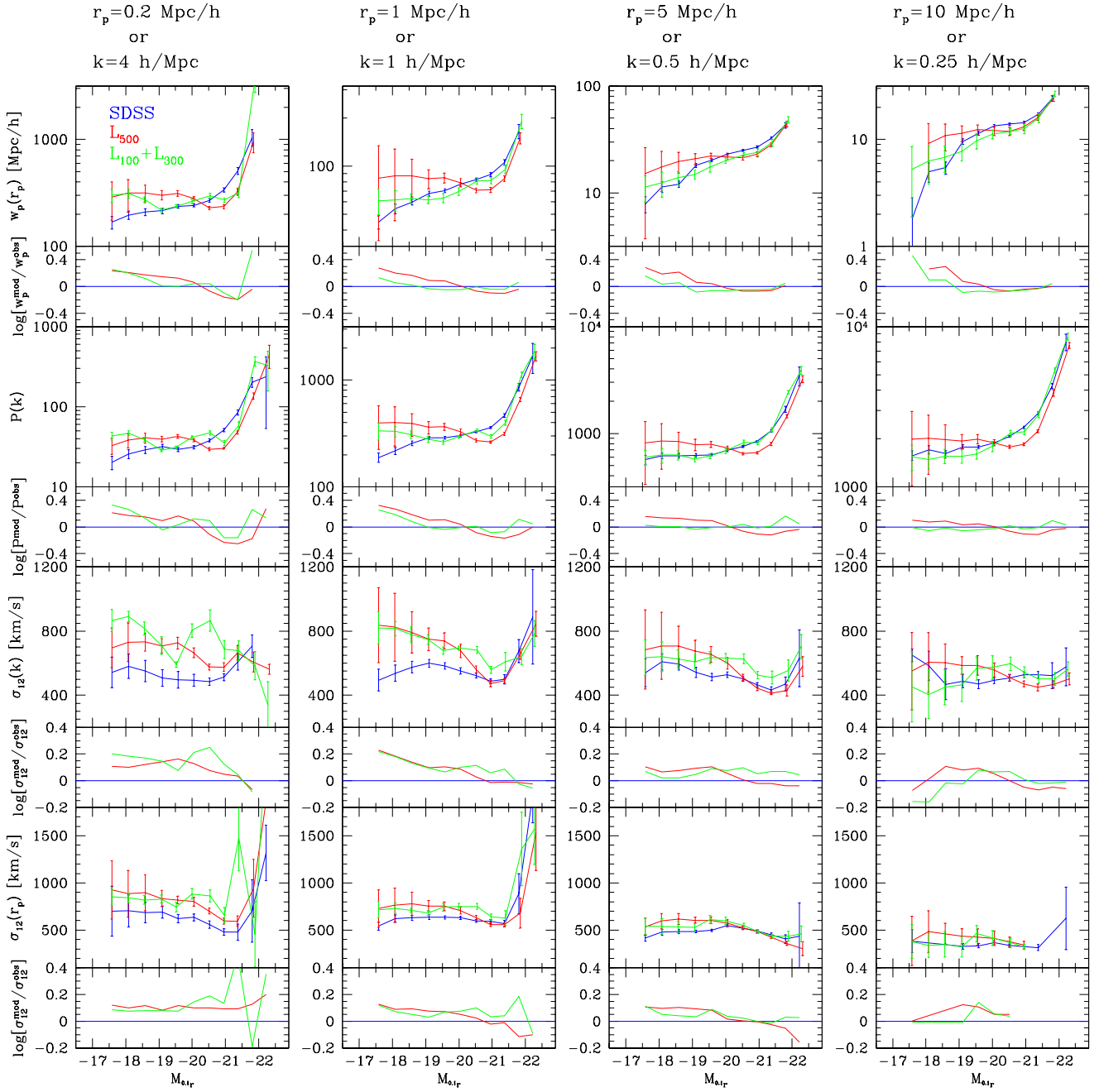


Figure 6. Clustering and velocity statistics as a function of luminosity on different scales, compared between model predictions and observations. Panels from left to right correspond to different projected separations r_p or scales k , as indicated above the top panels. Panels from top to bottom correspond to different statistics: $w_p(r_p)$, $P(k)$, $\sigma_{12}(k)$ and $\sigma_{12}(r_p)$. Blue and green lines are the model predictions respectively from the L_{500} and the $L_{100} + L_{300}$ mock catalogues, while blue lines are for the SDSS DR4 observations. The smaller panel below each bigger one plots the ratios of the model prediction to the observation. The PVDs measured at $k = 1 \text{ hMpc}^{-1}$ are also compared to the 2dFGRS result (black circles with error bars) presented by JB04.

measurements (blue lines in Figure 1) are plotted in this figure, also as blue lines. It should be pointed out that, for faint galaxies, the error bars on the $L_{100} + L_{300}$ curves are smaller than that on the L_{500} curves. This is because the faint galaxies are taken from the L_{100} box, which artificially reduces the cosmic variance.

It is seen that both models match the observations reasonably well. The agreement is better for the two-point cor-

relation function than for the PVD, and it is also better for more luminous galaxies. For galaxies brighter than -19, the models reproduce the $w_p(r_p)$ and $P(k)$ measurements on scales of $r_p > 1 \text{ h}^{-1}\text{Mpc}$ or $k < 1 \text{ hMpc}^{-1}$, but marginally overpredict or underpredict the clustering power on smaller scales in some cases. For galaxies fainter than -19, both models predict stronger clustering on all scales compared to the observations. It should be noted that the errors due to cos-

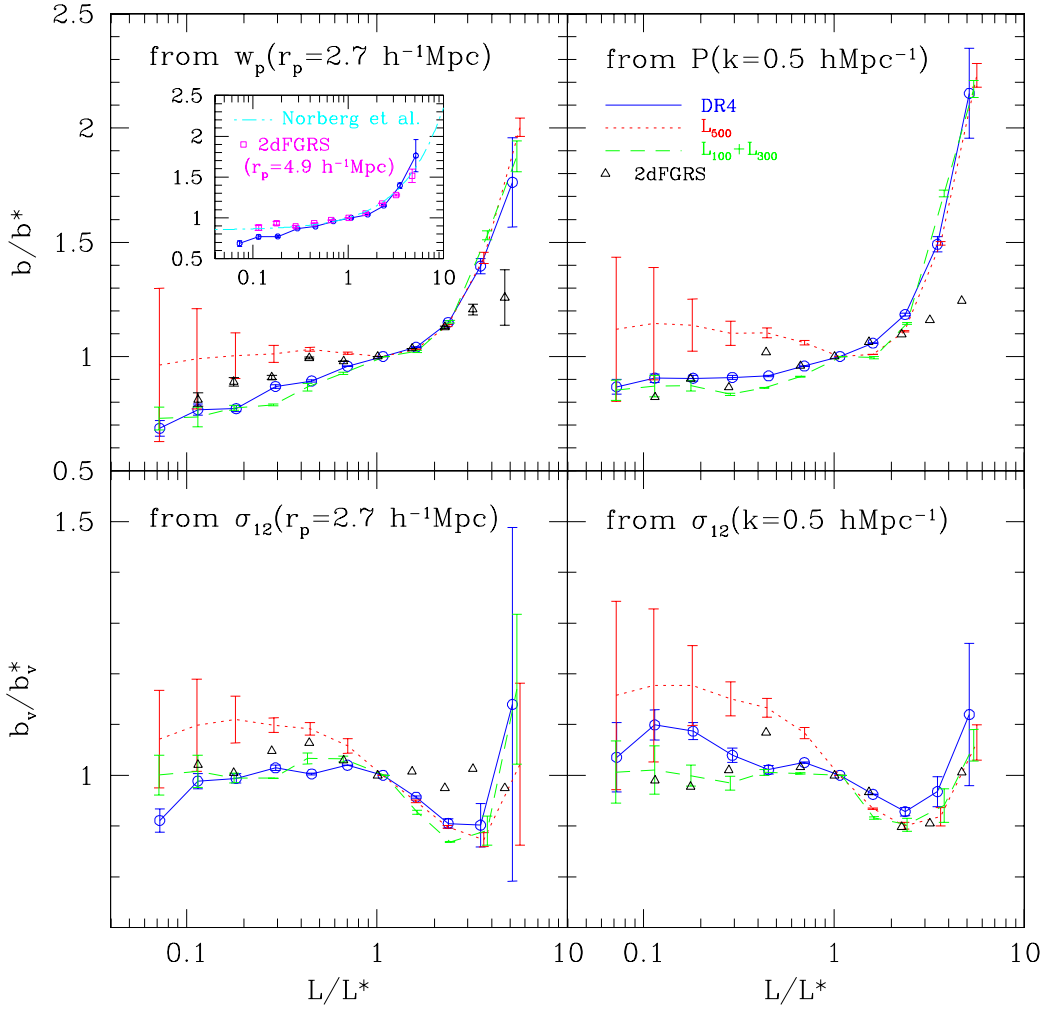


Figure 7. The spatial and velocity bias factors, scaled by their values at the characteristic luminosity L^* , as a function of the luminosity. The bias factors are estimated from the measurements of clustering/PVD at $r_p = 2.7 \text{ } h^{-1}\text{Mpc}$ or $k = 0.5 \text{ } h\text{Mpc}^{-1}$, as indicated in each panel. The green data points with error bars connected with dashed lines are for the model of Kang et al., and those in red connected with dotted lines are for the model of Croton et al.. The results from the SDSS are represented with the blue points with error bars connected with the solid lines. The open triangles are the 2dFGRS results from JB04. In the inset of the top panel at the left-hand, the squares with error bars are also from JB04 but are obtained using $w_p(r_p)$ at $r_p = 4.89 \text{ } h^{-1}\text{Mpc}$, and the dotted-dashed line is a fit to $w_p(r_p)$ measurements at $r_p = 4.89 \text{ } h^{-1}\text{Mpc}$ in the 2dFGRS $b/b^* = 0.85 + 0.15L/L^*$ given in (Norberg et al. 2001). For clarity, the error bars for the 2dFGRS results (open triangles), which are comparable to that in the top-left panel, are not plotted in the other panels.

mic variance are large so the disagreement is only marginally significant.

Similar result are found for the PVD. On scales of $r_p > 1 \text{ } h^{-1}\text{Mpc}$ or $k < 1 \text{ } h\text{Mpc}^{-1}$ and above $M_{0.1r} = -20$, both $\sigma_{12}(r_p)$ and $\sigma_{12}(k)$ are well matched by the models (especially the model of C06). For L^* galaxies (Sample L7 in Table 1), the PVD values predicted by the model of K05 are larger than those by C06, with the difference becoming more significant on small scales. This can be understood because K05 adopted in their model a larger value of Ω_m than C06. For faint galaxies, the discrepancy between the models and the observation seen in clustering statistics is also seen in the PVD. The model predictions are higher than the observations, but there are large uncertainties due to cosmic variance.

These results are shown more clearly in Figure 6,

where we have plotted $w_p(r_p)$ and $\sigma_{12}(r_p)$ at $r_p = 0.2, 1, 5, 10 \text{ } h^{-1}\text{Mpc}$, and $P(k)$ and $\sigma_{12}(k)$ at $k = 0.25, 0.5, 1, 4 \text{ } h\text{Mpc}^{-1}$, as a function of absolute magnitude. The ratios of the model predictions relative to the SDSS observations are also plotted. We see that both models match the observations for high-luminosity galaxies ($M_{0.1r} < -19$), but overpredict the clustering amplitude at low luminosities. The model of K05 better reproduces the clustering statistics, while the model of C06 more closely matches the PVD. Although the models predict higher pairwise velocities at faint luminosities than seen in the observations, it is still encouraging to see that the non-monotonic dependence of $\sigma_{12}(k)$ on luminosity is recovered by both models. This behaviour also exists in configuration space, but is less pronounced compared to Fourier space. This is qualitatively consistent with the HOD results of Tinker et al. (2006).

In the two top panels of Figure 7, we plot the bias of galaxies b as a function of luminosity; this has been done in many previous papers (e.g. Norberg et al. 2002; Tegmark et al. 2004; Zehavi et al. 2005; Paper I). Here the bias factor is normalised by its value at the characteristic luminosity M_* . In the top left panel, we estimate b using the projected 2PCF $w_p(r_p)$ at $r_p = 2.7 h^{-1}$ Mpc as in Zehavi et al. (2005). In the top right panel, we use $P(k)$ at $k = 0.5 h\text{Mpc}^{-1}$ to measure b . The prediction of K05 is in excellent agreement with the observations. C06 predicts too strong a bias for faint galaxies. In an analogous way, we plot the velocity bias b_v at $r_p = 2.7$ Mpc and $\sigma_{12}(k)$ at $k = 0.5 h\text{Mpc}^{-1}$ (bottom panels). This plot confirms that the non-monotonic behaviour found for $\sigma_{12}(k)$ at $k = 1 h\text{Mpc}^{-1}$ also exists at other scales ($k = 0.5 h\text{Mpc}^{-1}$) and in configuration space. Again we find that the model of K05 matches the observations very well, while the C06 model has a steeper luminosity dependence than observed. Note that when carrying out these comparisons, we have normalised the velocity bias by the value b_v^* at M_* . In fact, σ_{12} in the semi-analytic models is ~ 1.3 (K05) and ~ 1.1 (C06) times higher than in the observations (Fig.5). One possibility is that a CDM model with a lower value of $\Omega_m^{0.6} \sigma_8$ would fit the observational results better. However, as we will show in the next section, this is not required by the data.

Finally, it is interesting to compare measurements of the PVD from the SDSS and from the 2dFGRS, as this will indicate to what extent the observational results are still affected by variations between different regions of the sky. In Figure 7 the bias factors from the 2dFGRS calculated by JB04 are plotted as open triangles. From the figure, we see that there are small but significant differences with the SDSS results. For galaxies brighter than $2L^*$, the spatial bias is smaller in the 2dFGRS than in the SDSS. This is surprising because it has been claimed in the literature that there is no significant difference between the bias factors in the two surveys (e.g. Zehavi et al. 2005; Paper I). We note, however, that Zehavi compared her SDSS results with the 2dFGRS results of Norberg et al. (2001), where the $w_p(r_p)$ measurements were normalised at $r_p = 4.89 h^{-1}$ Mpc and not at $2.7 h^{-1}$ Mpc. We have gone back to the 2dFGRS data and we have estimated b using $w_p(r_p)$ at $r_p = 4.89 h^{-1}$ Mpc and we plot the results in Figure 7 as squares (the inset of the top-left panel). For comparison, the fitting function of Norberg et al. is plotted as a dotted-dashed line. As can be seen, our results calculated at $r_p = 4.89 h^{-1}$ Mpc are now perfectly consistent with Norberg et al., and are also in agreement with the SDSS results at high luminosities. This implies that the clustering properties of galaxies in the two surveys have a different dependence not only on luminosity, but also on scale. We have also studied the results at a variety of different scales. For example, when $r_p = 1 h^{-1}$ Mpc or $k = 1 h\text{Mpc}^{-1}$ is used for estimating b values, the two surveys are perfectly consistent with each other for galaxies brighter than -19 , but for fainter galaxies, both the spatial and the velocity biases are larger in the 2dFGRS than in the SDSS.

In spite of these complications, we find it encouraging that the semi-analytic models can reproduce the qualitative shape of the luminosity dependence at magnitudes $M_{0.1r} < -19$. It is not trivial to achieve this success. Pre-

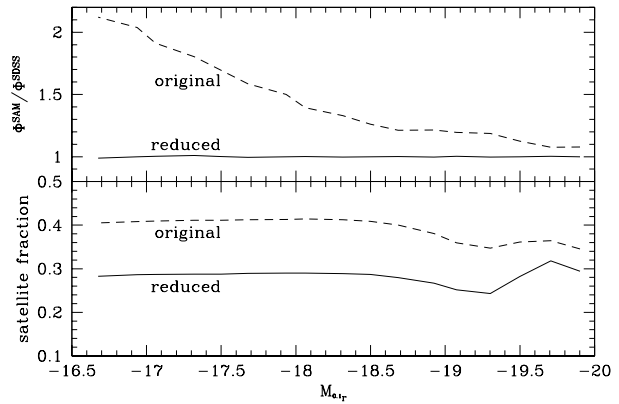


Figure 8. Top: the ratio of the luminosity function from the L_{500} model catalogue relative to that from the SDSS DR4. Bottom: the fraction of the satellite population in the same model catalogue. In both panels, the dashed (solid) line represents the result before (after) reducing the satellite fraction (see the text for details).

vious generations of semi-analytic models could not reproduce the strong increase of clustering at high luminosities (Kauffmann et al. 1999; Norberg et al. 2001). For faint galaxies, the clustering statistics are still not entirely reliable, because the surveys are still being affected by cosmic variance. Larger samples or better estimation methods are needed in order to make further progress.

5 ON THE DISCREPANCIES AT THE FAINT END

As we have seen in §4, there are some significant discrepancies between the observed PVD of faint galaxies and the result of the semi-analytic models. We have also seen (Figure 3) that both the C06 and K05 models overpredict the number of galaxies at the faint end of the luminosity function ($M_{0.1r} > -20$). This is the luminosity regime where the disagreement with the PVD data is worst. It is thus interesting to ask whether reducing the number of faint galaxies to provide a better match to the luminosity function would, at the same time, also solve the PVD discrepancy.

To answer this question, we have performed several simple mock experiments. In the first experiment, we randomly remove a number of faint galaxies with $M_{0.1r} > -20$ from the L_{500} model catalogue so that the resulting catalogue has the same ${}^{0.1}r$ -band luminosity function as the SDSS observations presented in Blanton et al. (2003b). When computing the luminosity function for the model catalogue, we have corrected the r -band absolute magnitude M_r of each model galaxy to its $z = 0.1$ value $M_{0.1r}$ in the same way as described in §3. We construct 10 mock catalogues using this reduced catalogue and we analyse the clustering and PVD in the same way as in §4. We find that the results are almost the same as presented in §4.

Since the PVD reflects the action of the local gravitational field, the discrepancies in the PVD at the faint end imply that the models predict too many faint galaxies that are located in high mass haloes. As we will see (Figure 12), these are mainly *satellite* systems rather than the central

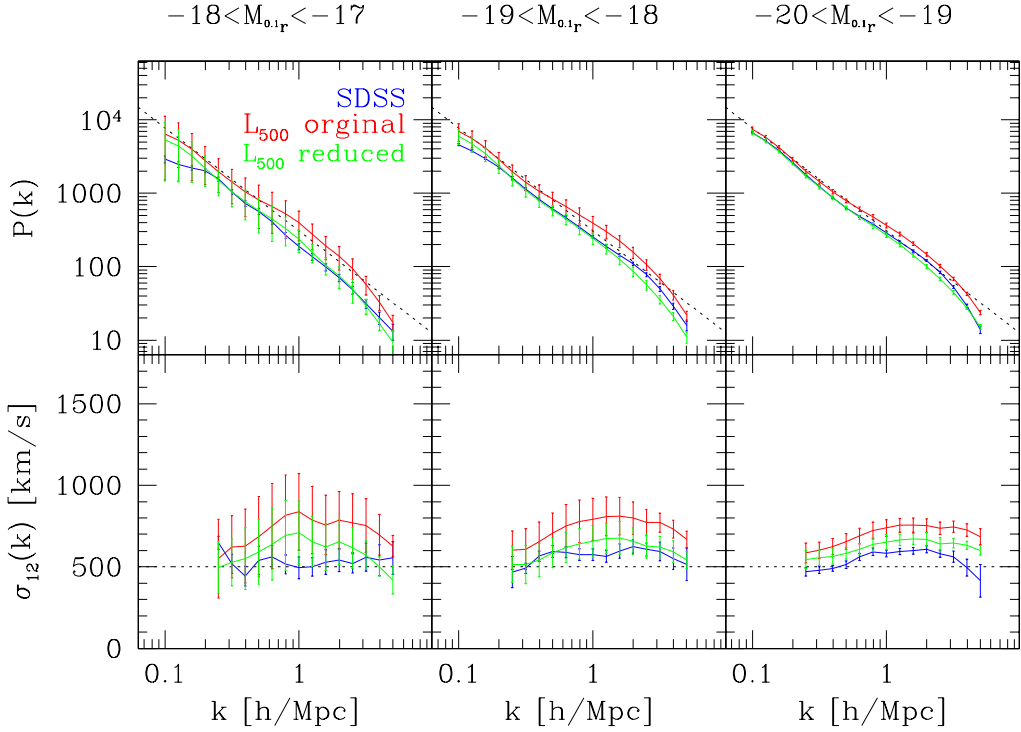


Figure 9. The power spectrum $P(k)$ (top panels) and the k -space PVD $\sigma_{12}(k)$ (bottom panels) obtained from the mock samples constructed based on the L_{500} model catalogue without (red) and with (green) the satellite fraction being reduced (see the text for details). The SDSS results are plotted in blue for comparison.

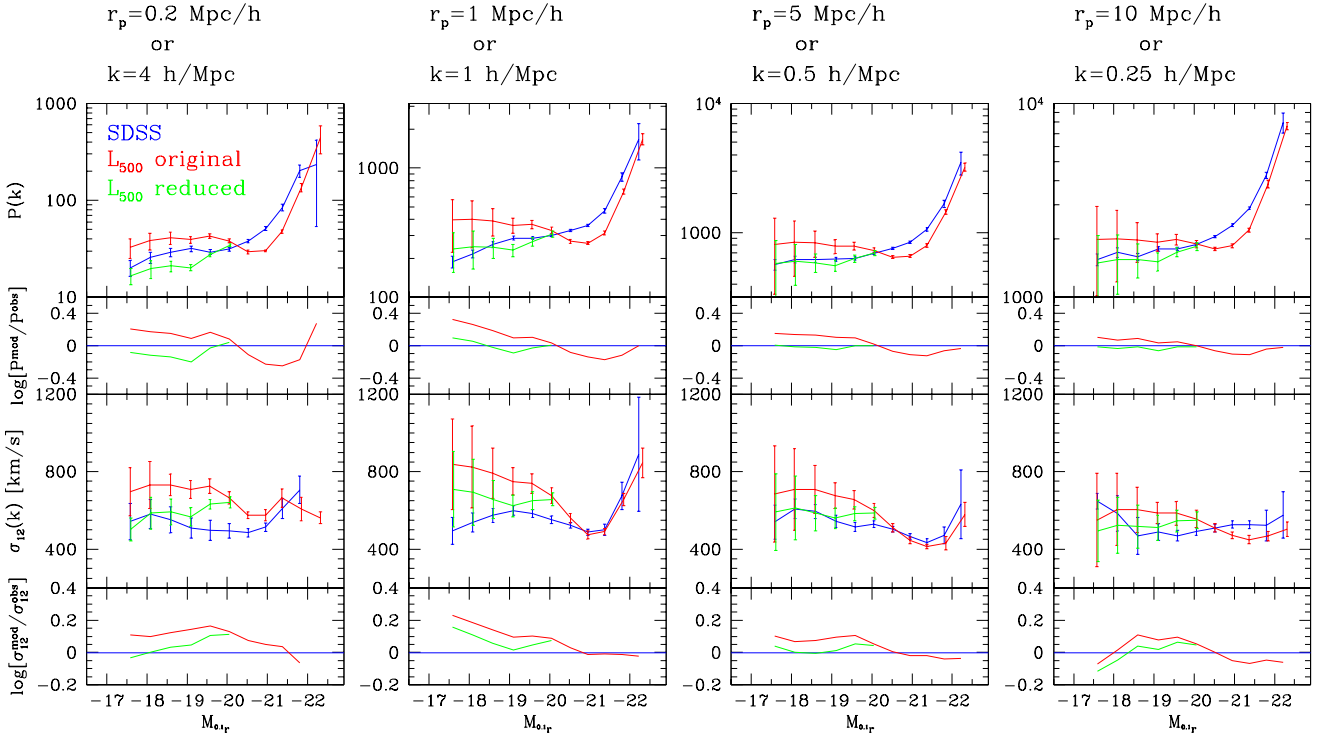


Figure 10. $P(k)$ and $\sigma_{12}(K)$ as a function of luminosity on different scales, compared between the mock samples constructed based on the L_{500} model catalogue without (red) and with (green) the satellite fraction being reduced (see the text for details). The SDSS results are plotted in blue for comparison. The smaller panel below each bigger one plots the ratios of the model prediction to the observation.

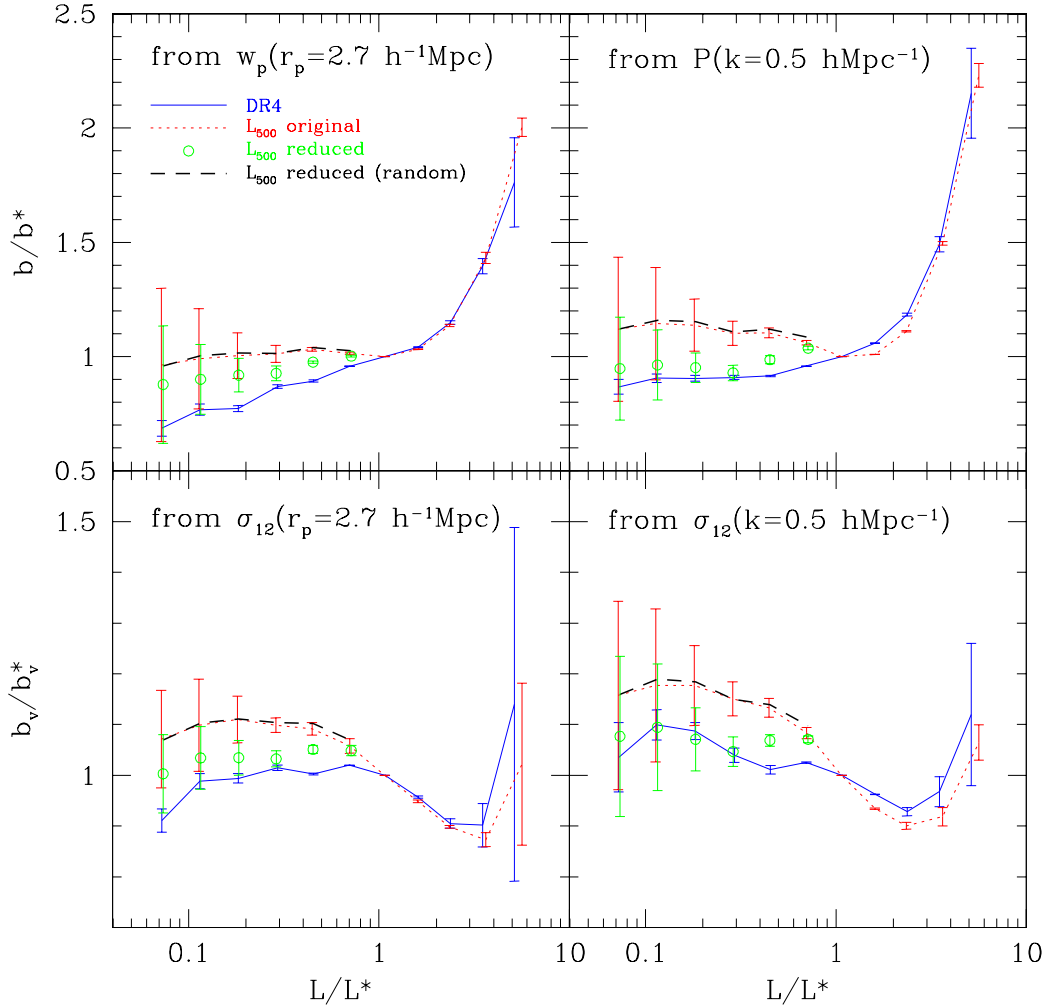


Figure 11. The spatial and velocity relative bias factor as a function of the luminosity, compared between the mock samples constructed based on the L_{500} model catalogue without (red) and with (green) the satellite fraction being reduced (see the text for details). The SDSS results are plotted in blue for comparison. The black dashed line is for the mock samples in which the total number of galaxies was reduced (to match the luminosity function) but the satellite fraction kept unchanged.

galaxies of their own halo. It is thus natural to speculate that it is these satellites that are responsible for the very large PVD values at low luminosities. We thus repeat the above experiment except that we preferentially eliminate satellites. Satellite galaxies with $M_{0.1r} > -20$ are randomly removed until the luminosity function comes into agreement with the observation, or until the fraction of satellite galaxies is reduced by more than 30%. In the latter case, we further remove a number of central galaxies at random so that the resulting catalogue has the same luminosity function as the observation.

Figure 8 compares the luminosity function and the satellite fraction for the original and the reduced model catalogues. Figure 9 compares the power spectrum $P(k)$ and the Fourier space PVD $\sigma_{12}(k)$ for the original (red) and the reduced (green) catalogues. The SDSS results are plotted in blue for comparison. Figure 10 plots $P(k)$ and $\sigma_{12}(k)$ at $k = 0.25, 0.5, 1, 4 \text{ } h\text{Mpc}^{-1}$, as a function of absolute magnitude. In Figure 11, we plot the results for the spatial and velocity bias factors. As can be seen from the three figures,

both the clustering power and the PVD for faint galaxies are reduced substantially and change to be consistent with the SDSS results. For comparison, we also plot in Figure 11 (dashed black lines) the bias factors obtained from the first experiment in which the number of faint galaxies is reduced at random, independent of whether it is a satellite or a central galaxy. As can be seen, there is almost no effect on the results. Finally we have also investigated what happens if we allow the fraction of satellite galaxies to be reduced by up to 50%. The agreement with observations is no longer very good; both the clustering amplitude and the peculiar velocities are now too small.

6 ON THE NON-MONOTONIC LUMINOSITY DEPENDENCE OF THE PVD

The non-monotonic luminosity dependence of PVD indicates that a substantial fraction of faint galaxies must reside in high-mass dark matter haloes. In paper II, we discussed

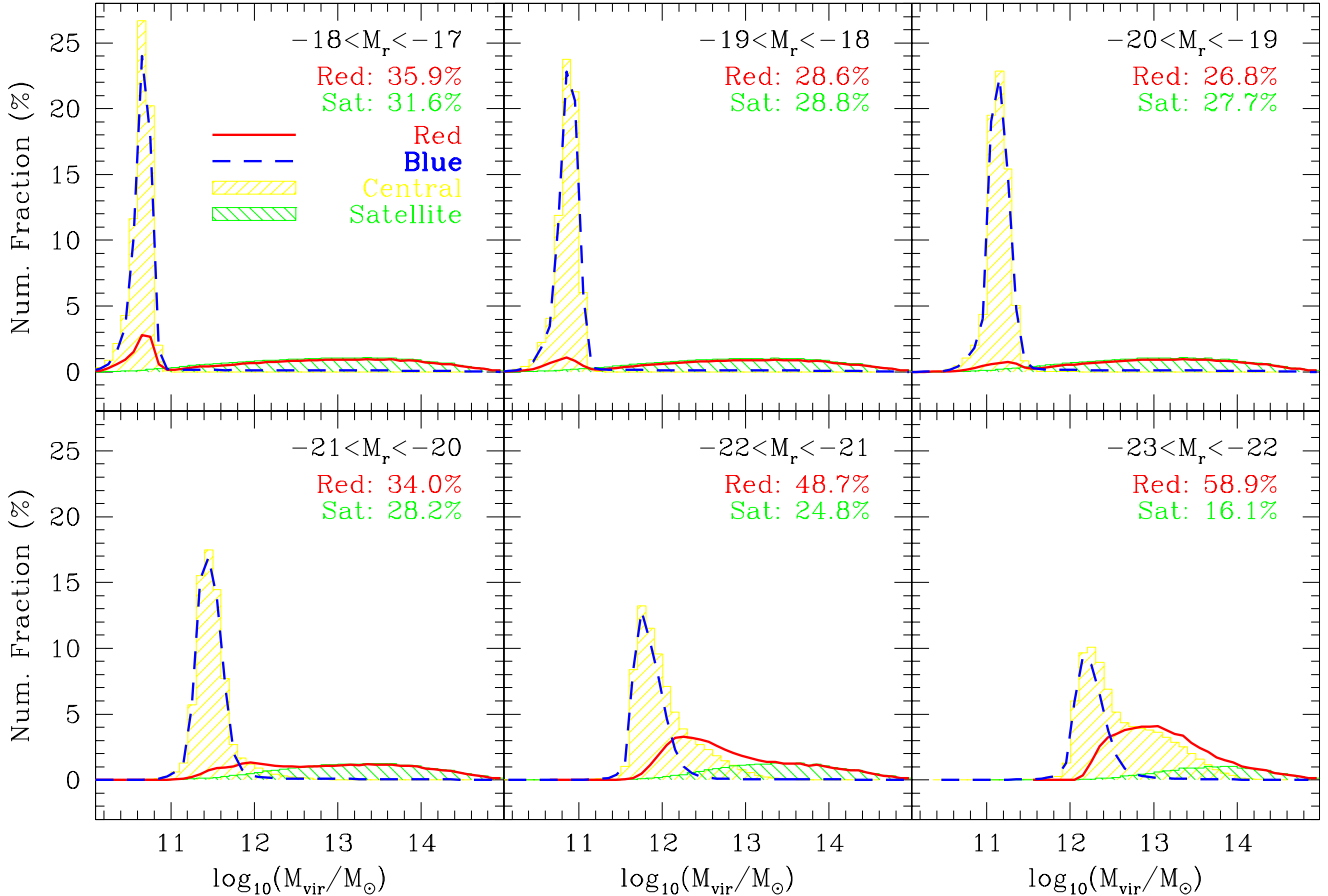


Figure 12. Distribution of the virial mass of host dark matter haloes for model galaxies in the reduced L_{500} catalogue in different luminosity intervals, as indicated in each panel. The red solid (blue dashed) lines represent the red (blue) galaxy population, and the yellow (green) shaded histogram shows the result for central (satellite) galaxies. The fraction of these populations are indicated in each panel.

how the faint red satellite galaxy population in dense environments, even though small in number, can still dominate the PVD on small scales ($k \sim 1 \text{ hMpc}^{-1}$). Here we use the galaxy catalogues from the semi-analytic models to check whether this hypothesis is correct.

We first divide the model galaxies in the *reduced* L_{500} catalogue into different luminosity intervals (we use rest-frame magnitudes for this analysis). We then divide each luminosity sample into red and blue subsamples using a luminosity-dependent colour cut, which is determined using the colour-magnitude diagram of galaxies in the L_{500} catalogue. The colour distribution is bimodal, so the natural place to divide the galaxies into "red" and "blue" subpopulations is at the minimum between the two peaks in the colour distribution.

Figure 12 shows the distribution of the virial mass of the host dark matter haloes for galaxies in different luminosity intervals. Red solid and blue dashed lines are for red and blue galaxies. The fraction of red and satellite populations are indicated in each panel. We also plot the results for central and satellite galaxies.

In each luminosity interval, the virial mass of host haloes shows a peak at lower masses and a longer tail to

higher masses. The position of the first peak moves to higher masses for more luminous galaxies. When the galaxies are divided into central and satellite systems, we see that the central galaxies dominate the first peak at low halo mass and the satellite galaxies are located in the tail of higher mass halos. This result may provide clues to understanding the bimodal colour distribution of galaxies. The fraction of satellite systems in high mass halos increases with decreasing galaxy luminosity up to $M_r \sim -19$, and then remains constant at around $\sim 30\%$ at fainter magnitudes. It is this satellite population that gives rise to a high PVD at the faint luminosities. In the models the satellites are mainly red and we note that the satellite fractions predicted by the models are in good agreement of the fraction of red galaxies observed in the SDSS (see Table 1 of Paper I).

7 SUMMARY

In this paper, we have compared the clustering and pairwise velocities for galaxies in different luminosity intervals measured from Sloan Digital Sky Survey with results from mock catalogues constructed using the semi-analytical models of

Kang et al. (2005) and Croton et al. (2006). We show that the models can match a number of key features of the luminosity dependence of the clustering and the PVD, including the monotonic increase of the clustering amplitude with luminosity and the non-monotonic behaviour of the PVD.

A direct look into the galaxy catalogues supports the conclusion that a substantial fraction of faint galaxies must reside in high mass dark matter haloes. The luminosity dependence of the PVD is mostly determined by how galaxies of different luminosities are distributed among/inside dark matter haloes. All these results are consistent with the recent studies of Slosar et al. (2006), Tinker et al. (2006) and van den Bosch et al. (2006) which were carried out using halo occupation distribution (HOD) models.

We have also identified a few significant differences between the models and the observations. The differences are generally at the level of a few tens of percent both in the clustering and in velocity statistics. One difference is that the PVD predicted by the models is systematically higher than the observations. Another difference is that the clustering of faint galaxies, especially in the C06 model, is significantly stronger than that observed in the SDSS. However, we note that cosmic variance effects are still significant at faint luminosities because the effective surveyed volume is small. Significant differences also still exist between the 2dFGRS and the SDSS clustering measurements. If this overprediction of the clustering for faint galaxies is confirmed, our experiment in §5 shows that the fraction of faint satellite galaxies in massive halos will have to be reduced by a factor of $\sim 30\%$ in order to bring the models into better agreement with the data. The recent study by Weinmann et al. (2006), which compares the fraction of central and satellite galaxies in dark halos between the C06 model and the SDSS, has found that the fraction of the faint galaxies is too high in massive halos. The strong clustering found here for faint galaxies in the model is clearly consistent with their findings.

ACKNOWLEDGMENTS

CL acknowledges the financial support by the exchange program between Chinese Academy of Sciences and the Max Planck Society. This work is supported by NSFC(10643005, 10373012, 10533030), by Shanghai Key Projects in Basic research (04jc14079, 05xd14019), and by the Max Planck Society.

The Millennium Run simulation used in this paper was carried out by the Virgo Supercomputing Consortium at the Computing Centre of the Max-Planck Society in Garching. The semi-analytic galaxy catalogue is publicly available at <http://www.mpa-garching.mpg.de/galform/agnpaper>.

Funding for the SDSS and SDSS-II has been provided by the Alfred P. Sloan Foundation, the Participating Institutions, the National Science Foundation, the U.S. Department of Energy, the National Aeronautics and Space Administration, the Japanese Monbukagakusho, the Max Planck Society, and the Higher Education Funding Council for England. The SDSS Web Site is <http://www.sdss.org/>. The SDSS is managed by the Astrophysical Research Consortium for the Participating Institutions. The Participating Institutions are the American Museum of Natural History, Astro-

physical Institute Potsdam, University of Basel, Cambridge University, Case Western Reserve University, University of Chicago, Drexel University, Fermilab, the Institute for Advanced Study, the Japan Participation Group, Johns Hopkins University, the Joint Institute for Nuclear Astrophysics, the Kavli Institute for Particle Astrophysics and Cosmology, the Korean Scientist Group, the Chinese Academy of Sciences (LAMOST), Los Alamos National Laboratory, the Max-Planck-Institute for Astronomy (MPIA), the Max-Planck-Institute for Astrophysics (MPA), New Mexico State University, Ohio State University, University of Pittsburgh, University of Portsmouth, Princeton University, the United States Naval Observatory, and the University of Washington.

REFERENCES

- Abel T., Anninos P., Zhang Y., Norman M. L., 1997, New Astronomy, 2, 181
- Adelman-McCarthy J. K., Agüeros M. A., Allam S. S., Anderson K. S. J., Anderson S. F., Annis J., Bahcall N. A., Baldry I. K., et al., 2006, ApJS, 162, 38
- Barrow J. D., Bhavsar S. P., Sonoda D. H., 1984, MNRAS, 210, 19P
- Berlind A. A., Weinberg D. H., 2002, ApJ, 575, 587
- Blanton M. R., Brinkmann J., Csabai I., Doi M., Eisenstein D., Fukugita M., Gunn J. E., Hogg D. W., et al., 2003a, AJ, 125, 2348
- Blanton M. R., Hogg D. W., Bahcall N. A., Brinkmann J., Britton M., Connolly A. J., Csabai I., Fukugita M., et al., 2003b, ApJ, 592, 819
- Blanton M. R., Lin H., Lupton R. H., Maley F. M., Young N., Zehavi I., Loveday J., 2003c, AJ, 125, 2276
- Blanton M. R., Schlegel D. J., Strauss M. A., Brinkmann J., Finkbeiner D., Fukugita M., Gunn J. E., Hogg D. W., et al., 2005, AJ, 129, 2562
- Boerner, G., Deng, Z.-G., Xia, X.-Y., & Zhou, Y.-Y., 1991, Ap&SS, 180, 47
- Bryan G. L., Cen R., Norman M. L., Ostriker J. P., Stone J. M., 1994, ApJ, 428, 405
- Budavári T., Connolly A. J., Szalay A. S., Szapudi I., Csabai I., Scranton R., Bahcall N. A., Brinkmann J., et al., 2003, ApJ, 595, 59
- Cen R., Ostriker J. P., 1993, ApJ, 417, 415
- Cole S., Aragon-Salamanca A., Frenk C. S., Navarro J. F., Zepf S. E., 1994, MNRAS, 271, 781
- Cole S., Lacey C. G., Baugh C. M., Frenk C. S., 2000, MNRAS, 319, 168
- Colless M., Dalton G., Maddox S., Sutherland W., Norberg P., Cole S., Bland-Hawthorn J., Bridges T., et al., 2001, MNRAS, 328, 1039
- Cooray A., 2006, MNRAS, 365, 842
- Cooray A., Sheth R., 2002, Phy. Rep., 372, 1
- Couchman H. M. P., Thomas P. A., Pearce F. R., 1995, ApJ, 452, 797
- Croton D. J., Springel V., White S. D. M., De Lucia G., Frenk C. S., Gao L., Jenkins A., Kauffmann G., et al., 2006, MNRAS, 365, 11
- Davis M., Efstathiou G., Frenk C. S., White S. D. M., 1985, ApJ, 292, 371
- Davis M., Geller M. J., 1976, ApJ, 208, 13

- Eisenstein, D. J. et al. 2001, AJ, 122, 2267
 Davis M., Peebles P. J. E., 1983, ApJ, 267, 465
 Fisher K. B., Davis M., Strauss M. A., Yahil A., Huchra J. P., 1994, MNRAS, 267, 927
 Fukugita M., Ichikawa T., Gunn J. E., Doi M., Shimasaku K., Schneider D. P., 1996, AJ, 111, 1748
 Goto T., Yamauchi C., Fujita Y., Okamura S., Sekiguchi M., Smail I., Bernardi M., Gomez P. L., 2003, MNRAS, 346, 601
 Gunn J. E., et al., 1998, AJ, 116, 3040
 Gunn J. E., et al., 2006, AJ, 131, 2332
 Hamilton A. J. S., 1993, ApJ, 417, 19
 Hawkins E., Maddox S., Cole S., Lahav O., Madgwick D. S., Norberg P., Peacock J. A., Baldry I. K., et al., 2003, MNRAS, 346, 78
 Hogg D. W., Finkbeiner D. P., Schlegel D. J., Gunn J. E., 2001, AJ, 122, 2129
 Ivezić Ž., et al., 2004, AN, 325, 583
 Jing Y. P., Börner G., 2001a, MNRAS, 325, 1389
 Jing Y. P., Börner G., 2004, ApJ, 617, 782
 Jing Y. P., Mo H. J., Boerner G., 1998, ApJ, 494, 1
 Jing Y. P., Suto Y., 2002, ApJ, 574, 538
 Kang X., Jing Y. P., Mo H. J., Börner G., 2002, MNRAS, 336, 892
 Kang X., Jing Y. P., Mo H. J., Börner G., 2005, ApJ, 631, 21
 Kang, X., Jing, Y. P., & Silk, J., 2006, ApJ, 648, 820
 Katz N., Gunn J. E., 1991, ApJ, 377, 365
 Kauffmann G., Colberg J. M., Diaferio A., White S. D. M., 1999, MNRAS, 303, 188
 Kauffmann G., Nusser A., Steinmetz M., 1997, MNRAS, 286, 795
 Kauffmann G., White S. D. M., Guiderdoni B., 1993, MNRAS, 264, 201
 Lacey C., Silk J., 1991, ApJ, 381, 14
 Li C., Kauffmann G., Jing Y. P., White S. D. M., Börner G., Cheng F. Z., 2006a, MNRAS, 368, 21
 Li C., Jing Y. P., Kauffmann G., Börner G., White S. D. M., Cheng F. Z., 2006b, MNRAS, 368, 37
 Li C., Kauffmann G., Wang L., White S. D. M., Heckman T. M., Jing Y. P., 2006c, MNRAS, 372, 457
 Loveday, J., Maddox, S. J., Efstathiou, G., & Peterson, B. A., 1995, ApJ, 442, 457
 Lupton R., Gunn J. E., Ivezić Ž., Knapp G. R., Kent S., Yasuda N., 2001, ASPC, 238, 269
 Madgwick D. S., Hawkins E., Lahav O., Maddox S., Norberg P., Peacock J. A., Baldry I. K., Baugh C. M., et al., 2003, MNRAS, 344, 847
 Marzke R. O., Geller M. J., da Costa L. N., Huchra J. P., 1995, AJ, 110, 477
 Mo H. J., Jing Y. P., Borner G., 1993, MNRAS, 264, 825
 Nagamine K., Springel V., Hernquist L., Machacek M., 2004, MNRAS, 350, 385
 Navarro J. F., White S. D. M., 1994, MNRAS, 267, 401
 Norberg P., Baugh C. M., Hawkins E., Maddox S., Peacock J. A., Cole S., Frenk C. S., Bland-Hawthorn J., et al., 2001, MNRAS, 328, 64
 Norberg P., Baugh C. M., Hawkins E., Maddox S., Madgwick D., Lahav O., Cole S., Frenk C. S., et al., 2002, MNRAS, 332, 827
 Peacock J. A., Smith R. E., 2000, MNRAS, 318, 1144
 Peebles P. J. E., 1980, The large-scale structure of the universe. Research supported by the National Science Foundation. Princeton, N.J., Princeton University Press, 1980. 435 p.
 Pier J. R., Munn J. A., Hindsley R. B., Hennessy G. S., Kent S. M., Lupton R. H., Ivezić Ž., 2003, AJ, 125, 1559
 Richards, G. T. et al. 2002, AJ, 123, 2945
 Schechter P., 1976, ApJ, 203, 297
 Seljak U., 2000, MNRAS, 318, 203
 Sheth R. K., Hui L., Diaferio A., Scoccimarro R., 2001, MNRAS, 325, 1288
 Slosar A., Seljak U., Tasitsiomi A., 2006, MNRAS, 366, 1455
 Smith J. A., et al., 2002, AJ, 123, 2121
 Somerville R. S., Davis M., Primack J. R., 1997, ApJ, 479, 616
 Somerville R. S., Primack J. R., 1999, MNRAS, 310, 1087
 Springel V., White S. D. M., Jenkins A., Frenk C. S., Yoshida N., Gao L., Navarro J., Thacker R., et al., 2005, Nature, 435, 629
 Springel V., White S. D. M., Tormen G., Kauffmann G., 2001, MNRAS, 328, 726
 Stoughton C., et al., 2002, AJ, 123, 485
 Strauss M. A., et al., 2002, AJ, 124, 1810
 Tegmark, M., et al. 2004, ApJ, 606, 702
 Thoul A. A., Weinberg D. H., 1995, ApJ, 442, 480
 Tinker J. L., Norberg P., Weinberg D. H., Warren M. S., 2006, astro, arXiv:astro-ph/0603543
 Tucker D. L., et al., 2006, AN, 327, 821
 van den Bosch F. C., Yang X., Mo H. J., 2003, MNRAS, 340, 771
 van den Bosch F. C., et al., 2006, astro, arXiv:astro-ph/0610686
 Weinberg D. H., et al. 1998, in Woodward C. E., Shull J. M., Thronson H. A., eds, ASP Conf. Ser. 148: Origins Simulating Cosmic Structure Formation. pp 21–+
 Weinmann S. M., van den Bosch F. C., Yang X., Mo H. J., Croton D. J., Moore B., 2006, /mnras, 372, 1161
 White S. D. M., Frenk C. S., 1991, ApJ, 379, 52
 Xia, X. Y., Deng, Z. G., & Zhou, Y. Y., 1987, IAU Symp. 124: Observational Cosmology, 124, 363
 Yan R., Madgwick D. S., White M., 2003, ApJ, 598, 848
 Yan R., White M., Coil A. L., 2004, ApJ, 607, 739
 Yang X., Mo H. J., Jing Y. P., van den Bosch F. C., Chu Y., 2004, MNRAS, 350, 1153
 Yang X., Mo H. J., van den Bosch F. C., 2003, MNRAS, 339, 1057
 York D. G., Adelman J., Anderson Jr. J. E., Anderson S. F., Annis J., Bahcall N. A., Bakken J. A., Barkhouser R., et al., 2000, AJ, 120, 1579
 Yoshikawa K., Jing Y. P., Suto Y., 2000, ApJ, 535, 593
 Zehavi I., Blanton M. R., Frieman J. A., Weinberg D. H., Mo H. J., Strauss M. A., Anderson S. F., Annis J., et al., 2002, ApJ, 571, 172
 Zehavi I., Zheng Z., Weinberg D. H., Frieman J. A., Berlind A. A., Blanton M. R., Scoccimarro R., Sheth R. K., et al., 2005, ApJ, 630, 1
 Zurek W. H., Quinn P. J., Salmon J. K., Warren M. S., 1994, ApJ, 431, 559

This paper has been typeset from a Te_X/La_Te_X file prepared by the author.